JOURNAL OF PROPULSION AND POWER
Vol. 19, No. 1, January–February 2003

Sensitivity of Hydrocarbon Combustion Modeling for Hypersonic Missile Design

Ryan P. Starkey* and Mark J. Lewis†
University of Maryland, College Park, Maryland 20742

Aspects relating to the aerodynamic and propulsive design and analysis of missile-class, waverider-based hypersonic vehicles are explored in this paper. A quasi-one-dimensional engine model, including the effects of fuel injection, mixing, chemical production rates, heat transfer, and viscous losses, is developed and utilized to assess the effects of finite rate, hydrocarbon chemistry on optimized missile configurations. Resultant optimized single- and double-engine missile designs are shown for changes in fuel mixing length, fuel mixing efficiency, fuel-injector location, and assumed fuel mass fraction. The effects of these different design conditions on the cruise range are explored, as well as perturbations around these design points for optimized vehicles. Missiles are optimized for steady-state trim conditions at the beginning of cruise flight using parallelized genetic algorithm optimization software developed for this study. All missile designs are assumed to reach cruising altitude and velocity through the use of an external rocket booster. The missile is geometrically constrained to fit within the 0.61 × 0.61 × 4.27 m box limits for a naval vertical launch tube and has a desired cruise range of 750 km at Mach 8. Results show that the optimized combustor designs were extremely sensitive to small design perturbations. Two engine configurations are shown to be more robust than single-engine models for engine design perturbations.

Nomenclature

A	=	combustor area, m^2
a	=	acceleration, m/s^2
a, b, c, d, f	=	fuel-injection constants
C	=	coefficient
D	=	drag, N; hydraulic diameter, m
h	=	height, m; enthalpy, J/kg
I_{sp}	=	specific impulse, s
I_y	=	mass moment of inertia, kg · m^2
L	=	lift, N; length, m
M	=	Mach number, moment, N · m
MW	=	molecular weight, kg/mole
m	=	mass, kg
$\dot{m}$	=	mass flow rate, kg/s
Pr	=	Prandtl number
p	=	pressure, N/m^2
$\dot{Q}$	=	heat flux, W
R	=	range, km; radius, m
Re	=	Reynolds number
$\bar{r}$	=	normalized radius
S	=	area, m^2
T	=	thrust, N; temperature, K
t	=	plate thickness, m
U	=	velocity, m/s
V	=	volume, m^3
W	=	weight, N
X	=	injector locations, m
x, y, z	=	coordinate directions
Y	=	species mass fractions
Z	=	altitude, km
α	=	combustor function
β	=	shock angle, deg
γ	=	ratio of specific heats
η	=	efficiency
θ	=	compression surface angle, deg
κ	=	fuel volume fraction
π	=	fuel mass fraction
ρ	=	density, kg/m^3
ϕ	=	equivalence ratio
ω	=	angular acceleration, rad/s^2
$\dot{\omega}$	=	chemical production rate, kg/s

Subscripts

a	=	air
added	=	incremental addition to combustor
aw	=	adiabatic wall
box	=	box efficiency
C_g	=	center of gravity
c	=	cone
cap	=	capture area
cen	=	centrifugal
e	=	end of injection; edge of boundary layer
f	=	fuel; friction
i	=	individual species
inj	=	injection
mix	=	fuel mixing and burning efficiency
o	=	total condition
p	=	pressure; specific heat at constant pressure
s	=	structure; start of injection
T	=	transition
tung	=	tungsten
v	=	viscous
x	=	translational direction
w	=	wave drag; wetted surface area; wedge
z	=	vertical direction
∞	=	freestream value

Received 8 October 2001; revision received 30 April 2002; accepted for publication 30 June 2002.

*Faculty Research Scientist, Department of Aerospace Engineering; rstarkey@eng.umd.edu. Member AIAA.

†Professor, Department of Aerospace Engineering; lewis@eng.umd.edu. Associate Fellow AIAA.

Introduction

WHEN designing waverider-integrated hypersonic cruise vehicles, the general approach is to maximize the lift-to-drag ratio (L/D) while guaranteeing sufficient internal volume for payload, fuel, landing gear, avionics, and possibly crew cabin. For a missile-scale waverider-based vehicle the design considerations are

considerably different; the aerodynamic performance and volume considerations (structural, fuel, and payload) must be coupled to the necessity of fitting within the highly constrictive launch shroud. Satisfying the external constraints becomes even more difficult for nonaxisymmetric missile configurations, such as the waverider designs presented. The consideration of the internal and external geometric constraints, the desired missile range, and the extremely nonlinear design space creates a difficult optimization problem that can only be resolved through high-fidelity vehicle modeling and sophisticated optimization techniques. This difficulty, in part, is caused by the relatively small magnitude of the net forces involved (i.e., positive lifting forces can be 20 times the weight, whereas negative lifting forces are 19 times the weight to result in lift equal to weight).

Although it has long been known that the effects which finite rate chemistry would have on the optimization of a vehicle design are significant, the complexity of incorporating this type of computation into an optimization process (with a realistic computational time) were overwhelming. This fact is further complicated by the large number of chemical species and reactions required to analyze the combustion mechanisms for large hydrocarbon molecules. With the advent of newer high-speed computers, along with the implicit parallelization ability of genetic algorithms, the feasibility of including finite rate chemistry in an optimization process is possible. Nevertheless, the computational expense for optimization of this type is still considerable.

Because these missiles are essentially flying engines, the outcome (i.e., accuracy) of the design and analysis of the supersonic combustion ramjet (scramjet) engine has more influence on the performance of the missile than any other system. Unfortunately, the combustor is also the most complex component to analyze correctly. The analysis is further complicated by fuel injection and mixing, starting and unstarting considerations, energy-exchange mechanisms (combustion and heat transfer), wall-cooling problems, shock and boundary-layer ingestion, shock-boundary-layer interactions, pressure vessel mechanics, unsteady combustion, piloting, flameholding, and numerous other problems. It is not realistic to attempt to model most of these phenomena, especially in an optimization process. In the combustor model presented, some of these issues are dealt with; however, most are not. The issues investigated are ones on which there is considerable uncertainty as to what the correct magnitudes and configurations are, such as required inlet conditions, fuel injection and mixing lengths, combustion modeling, and required engine dimensions. Of course, by setting these parameters the resulting missile geometry is mostly fixed because of the maximum dimensional allowances of naval vertical launch tubes ($0.61 \times 0.61 \times 4.27$ m). Previous missile design work without the use of finite rate chemistry was presented by Starkey and Lewis.[1]

Aerodynamic Model

Example single- and double-engine missile designs are shown in Figs. 1 and 2, respectively, and can be referred to for understanding

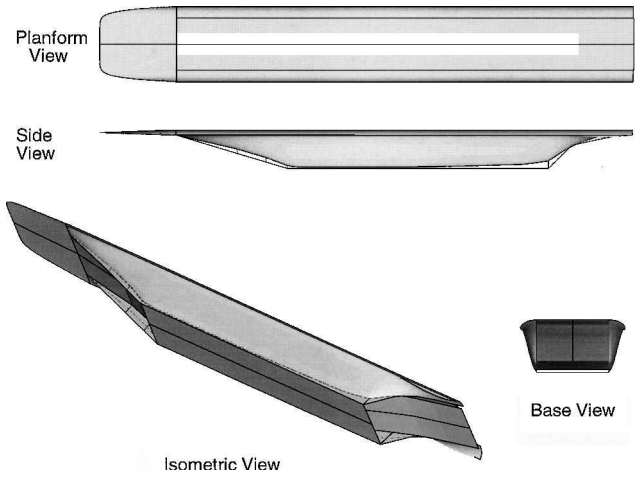

Fig. 1 Example optimized single-engine missile configuration.

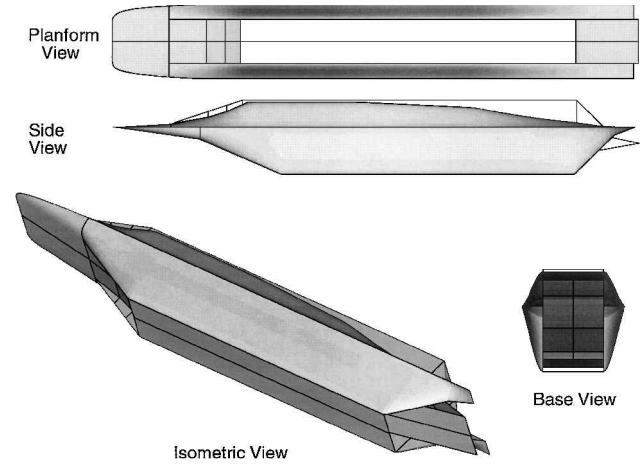

Fig. 2 Example optimized double-engine missile configuration.

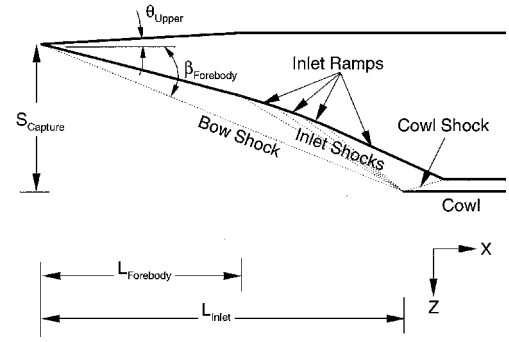

Fig. 3 Inlet geometry and shock system along the keel line for single engine missiles.

throughout this modeling section. The flowpath in these figures is from left to right. As shown in the example vehicles, the missile keel-line geometries consist of a waverider forebody, a multiple planar-ramp inlet compression system, a scramjet engine, and a half-plug nozzle.

Waverider geometries (conceived of by Nonweiler[2] in 1959) are inversely defined to have a bow shock attached everywhere to a sharp leading edge, thereby generating high values of L/D at high lift coefficient. The containment of compressed air between the attached leading-edge shock wave and the vehicle lower surface generates the high lift-to-drag ratios, as well as, a well-behaved flowfield for delivery into a two-dimensional airbreathing engine. A secondary benefit of leading-edge shock attachment is the minimization of the amount of energy required for precompressing air for combustion (i.e., shallower shock angles). Extensive work has been spent studying and validating these waverider characteristics theoretically,[3] computationally,[4] and experimentally.[5] The coupling between forebody and combustor becomes even more significant for this missile application as a result of the high inlet pressures and temperatures needed to combust a hydrocarbon fuel in the length restricted engine.

A waverider-based forebody is generated using the analytical variable wedge angle (VWA) method.[6,7] The VWA method was shown to provide the same results as higher-order methods in orders of magnitude less time, thereby providing an ideal forebody model for an optimization process. Although restricted to being two-dimensional for the width of the engine, the VWA model generates a configuration with a three-dimensional shock structure. Single-engine missile designs use compression on the upper surface of the forebody to aid in mitigating any excess lift and trimming out any moment about the center of gravity. A schematic of the inlet configuration is shown in Fig. 3. Forebodies of double-engine configurations are generated by combining the lower surfaces of two different forebody designs.[8]

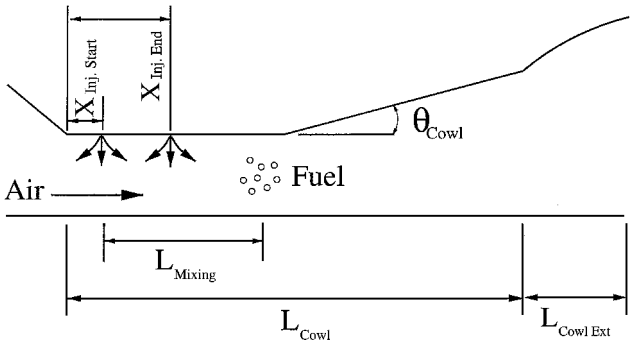

Fig. 4 Example scramjet configuration.

Following the forebody, for the width of the engine(s), are a series of between one and three successive compression ramps to create the inlet system. The shocks created by the forebody and compression ramps are all designed to converge at the cowl lip to maximize air mass capture for the engine(s), as shown in Fig. 3. The engine height is set so that the turning shock off of the cowl lip is canceled at an expansion corner at the end of the last inlet ramp. Therefore, the inlet geometry directly defines the engine dimensions, inlet properties, and air mass flow rates. By allowing the vehicle height and number of inlet ramps to vary, these important engine conditions can be altered to suit the needs of the design in question. Double-engine missiles are not constrained to have the same ramp angles or number of ramps between the engine different engine flow paths, although a common engine width is used to simplify control surface integration (as explained next). Multiple-engine configurations are created by using the forebody model as just described followed by the two independent keel lines, as shown by the side view of the example missile in Fig. 2.

The combustor is designed to be constant area for half of the length and to have a diverging section for the remaining half. The angle for the diverging section is held constant, but allowed to differ between designs and engines. This diverging section allows the engine inlet height to be smaller than a constant-area channel. By allowing an increase in cross-sectional area of the engine, additional heat can be released into the flow while avoiding thermal choking. Within the engine the starting and ending positions of the fuel injectors, as well as the mixing length of the fuel, are set by the variables X_{inj_s}, X_{inj_e}, and L_{mix}, respectively. The engine configuration details are shown in Fig. 4.

In the conception and formulation of this problem, it was deemed necessary to minimize the possibility of mechanical failures, and thus, the option of using deployable control surfaces was eliminated. To have effective pitch control, these missile designs incorporate a portion of the trailing edge of the nozzle(s) as a control surface. The nozzle trailing edge was considered to be the best place to include the control surface because the pressures at this point are relatively low, but higher than freestream, and contribute little to the thrust of the vehicle (i.e., primarily lifting forces; caused by the nozzle curvature). The nozzle wall, defined by a second-order polynomial ($y = Ax^2 + Bx + C$), is created such that there is an internal nozzle followed by an external half-plug nozzle. For simplicity, the nozzle flowfield is calculated using the two-dimensional method of characteristics,[9] assuming the control surface is not deflected. A centered expansion fan or oblique shock approximation is then applied as a first-order correction to the properties along a deflected control surface.

The airframe (everything excluding the engine flowpath) is analyzed using a modified shock-expansion method, which was developed for this study.[8] Shock-expansion theories[10] are inaccurate for this application because they determine the flowfield using Prandtl–Meyer theory (hypersonic slender body theory) assuming two-dimensional streamlines. Because of the highly curved nature of these missile airframes (i.e., three-dimensional flowfield), the shock-expansion method resulted in an overprediction in peak surface pressure by as much as 50%. The modified method uses a combination of the oblique shock relations and Taylor–Maccoll cone flow equations[11] to solve the local flow properties (for compression) while marching down "two-dimensional" streamlines. As with shock-expansion theory, the local flow conditions at a point and the relative inclination angle are used to calculate the properties at the next point. The blending of the properties predicted by the oblique shock and Taylor–Maccoll methods is based on the local radius of curvature in the spanwise direction. This blending method attempts to simply predict the pressure-relieving effects a three-dimensional body has on a two-dimensional streamline approximation to local flow conditions. Expansion regions are calculated using traditional shock-expansion theory.

The local radius of curvature R is determined in the spanwise plane

$$R = [1 + (y')^2]^{\frac{3}{2}} \Big/ |y''| \tag{1}$$

with allowable values (for these missiles) between 0 and 1 m. Any values ≥ 1 m are assigned a value of 1 m because in the limit of infinite radius of curvature cone flow degrades to wedge flow (i.e., for the purposes of this study, 1 m is assumed to be infinite because of the extremely small vehicle width limitation). The radius R is then normalized by a characteristic radius of 1 m (empirical to these missile geometries and scales) resulting in $\bar{r} \equiv R/1$ m. The actual surface properties for compression surfaces are then found by linear interpolation

$$\begin{bmatrix} p \\ T \\ M \end{bmatrix} = \bar{r} \begin{bmatrix} p_w \\ T_w \\ M_w \end{bmatrix} + (1 - \bar{r}) \begin{bmatrix} p_c \\ T_c \\ M_c \end{bmatrix} \tag{2}$$

where $()_w$ are wedge-flow values calculated from oblique-shock theory and $()_c$ are conical-flow values determined from solution to the Taylor–Maccoll equations. Results using this methodology have been validated using Euler computational fluid dynamics (CFD) calculations for optimized single- and double-engine missile configurations.[8] The front half of a single-engine missile is shown in Fig. 5 with the corresponding analytical and CFD pressure (atm) results shown in Fig. 6. The analytical model shown in Fig. 6 has both the forebody and the side airframe, whereas the CFD solution only shows the side of the of the forebody that connects to the side airframe. Calculations were carried out in this manner to simplify grid generation because CFD solutions of the forebody alone demonstrated that the streamlines were in fact two-dimensional for the keel-line portion. Using the two-dimensional shock-expansion method, the peak pressure of 1.05 atm was generated at the side of the engine; with the modified shock-expansion method the peak pressure was 0.66 atm with under 1% error when compared to the Euler CFD calculations.

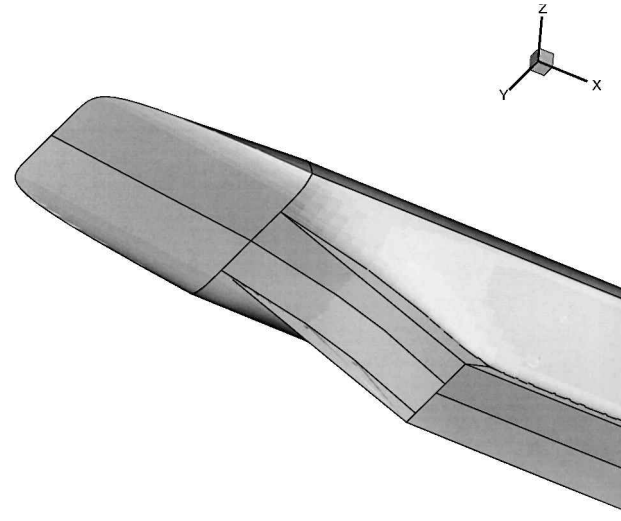

Fig. 5 Single-engine missile validation model (front half).

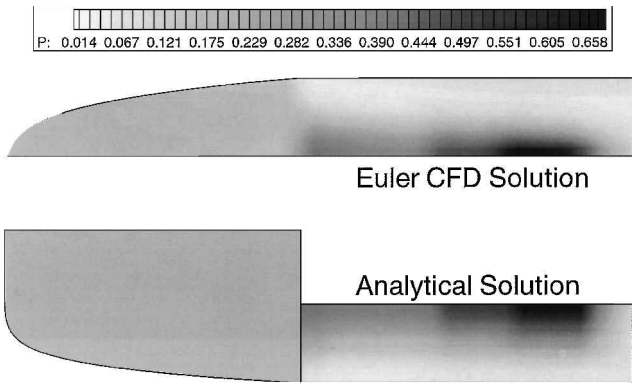

Fig. 6 Modified shock-expansion method validation (pressure contours).

Viscous drag is calculated with the reference temperature method[12] using Eckert's empirical estimate for the average boundary-layer temperature. To keep the model simple, a single estimate for the wall temperature of 1200 K is used over the entire vehicle. Dynamic viscosity at the reference temperature is approximated by Sutherland's law.[12] An empirical correlation by Bowcutt et al.[13] for the transition Reynolds number Re_T was used in this study.

$$\log_{10}(Re_T) = 6.421 \exp\left[1.209 \times 10^{-4} M_e^{2.641}\right] \tag{3}$$

was used for this study. The correlation shown in Eq. (3) is based on cone flow transition data. For most of the configurations generated in this study, the transition region was near the leading edge, resulting in a mostly turbulent boundary layer.

Structural Model

To concentrate on aerodynamic and propulsive effects and keep the structural analysis straightforward yet within reason, some approximations have been made for the mass distribution and structural/fuel volumes. The missiles have an assumed fuel volume fraction κ of the interior volume V. The structure is assumed to be a constant density shell of tungsten ($\rho_{\text{tung}} = 19{,}255$ kg/m^3) with a plate thickness of 3.17 mm. Assuming κ is a fraction of the interior of the tungsten shell and using Jet-A fuel ($\rho_f = 940$ kg/m^3) results in an approximate missile weight of

$$W = g[S_w t_{\text{tung}}(\rho_{\text{tung}} - \kappa\rho_f) + \kappa V \rho_f] \tag{4}$$

Because of the uncertainty of what value should be used for the fuel volume fraction κ, cases are examined with values of either 25 or 50%. This parameter was deemed important because different configurations will have different usable volumes. As the vehicle volume is increased, the volumes of the payload, avionics, pumps, etc. should remain relatively constant, thereby allowing more useful volume for fuel. Tungsten was chosen because of its large density to account for the mass of any payload, avionics, and other subsystems that might be present. Missiles created using these approximations have weights on the same order of magnitude as those created for the SCRAM missile program,[14] for which $\kappa \approx 35\%$.

Combustor Model

To capture all of the desired variations in the combustor geometry and their associated effects on the chemistry, a quasi-one-dimensional model was developed by O'Brien et al.[15] with partial basis on derivations given by Shapiro[16] and Turns.[17] Allowances were made to accommodate for variable cross-sectional area, include the effects of friction using a hydraulic diameter approximation, include the effects of heat transfer with the wall, and allow for the inclusion of a mixing profile, which increments the amount of combustible fuel. The general equation set is given by

$$\frac{1}{\rho}\frac{\mathrm{d}\rho}{\mathrm{d}x} + \frac{1}{U}\frac{\mathrm{d}U}{\mathrm{d}x} + \frac{1}{A}\frac{\mathrm{d}A}{\mathrm{d}x} = \frac{1}{\dot{m}}\frac{\mathrm{d}\dot{m}}{\mathrm{d}x} \tag{5}$$

$$\frac{1}{p}\frac{\mathrm{d}p}{\mathrm{d}x} + \frac{\gamma M^2}{2U^2}\frac{\mathrm{d}U^2}{\mathrm{d}x} + \frac{\gamma M^2}{2}\left(\frac{4C_f}{D}\right) + \frac{\gamma M^2}{\dot{m}}\frac{\mathrm{d}\dot{m}}{\mathrm{d}x} = 0 \tag{6}$$

$$\frac{\mathrm{d}Y_i}{\mathrm{d}x} = \frac{\dot{\omega}_i M W_i}{\rho U} - Y_i\frac{1}{\dot{m}}\frac{\mathrm{d}\dot{m}}{\mathrm{d}x} + \left[\frac{1}{\dot{m}}\frac{\mathrm{d}\dot{m}_i}{\mathrm{d}x}\right]_{\text{added}} \tag{7}$$

$$c_p\frac{\mathrm{d}T}{\mathrm{d}x} + \sum_i h_i\frac{\mathrm{d}Y_i}{\mathrm{d}x} = -U\frac{\mathrm{d}U}{\mathrm{d}x} - \frac{h_o}{\dot{m}}\frac{\mathrm{d}\dot{m}}{\mathrm{d}x} - \frac{1}{\dot{m}}\frac{\mathrm{d}[\dot{Q}''A]}{\mathrm{d}x} + \frac{1}{\dot{m}}\left[\sum_i \dot{m}_i C_{p_i}\frac{\mathrm{d}T}{\mathrm{d}x} + \sum_i \dot{m}_i h_i\frac{\mathrm{d}Y_i}{\mathrm{d}x} + \sum_i h_i\frac{\mathrm{d}\dot{m}_i}{\mathrm{d}x}\right]_{\text{added}} \tag{8}$$

$$\frac{1}{p}\frac{\mathrm{d}p}{\mathrm{d}x} = \frac{1}{\rho}\frac{\mathrm{d}\rho}{\mathrm{d}x} + \frac{1}{T}\frac{\mathrm{d}T}{\mathrm{d}x} - \frac{1}{\overline{MW}}\frac{\mathrm{d}\overline{MW}}{\mathrm{d}x} \tag{9}$$

$$\frac{\mathrm{d}\overline{MW}}{\mathrm{d}x} = -\overline{MW}^2\sum_i \frac{1}{MW_i}\frac{\mathrm{d}Y_i}{\mathrm{d}x} \tag{10}$$

where Eq. (5) is the conservation of mass, Eq. (6) is conservation of momentum in the x direction, Eq. (7) is the conservation law for each species involved, Eq. (8) is the conservation of energy, Eq. (9) is the equation of state, and Eq. (10) is the conservation of molecular weight. The $()_{\text{added}}$ terms represent incremental fuel addition terms to account for staggered mixing ports, fuel availability for combustion, or injection of combinations of various fuels and/or piloting agents. The variables Y_i, $\overline{MW}$, $\dot{Q}''$, $\dot{\omega}_i$, and U represent molecular mass fraction, average molecular weight, wall heat flux, chemical production rates, and velocity, respectively.

The values for area change $\mathrm{d}A/\mathrm{d}x$, incremental mass addition $\mathrm{d}\dot{m}/\mathrm{d}x$, and wall heating $\mathrm{d}[\dot{Q}''A]/\mathrm{d}x$ are all assumed to be known and are used as inputs to solve the following system of equations. The system has five plus i equations (where i is the number of species) and the same number of unknowns; it is solved in the form:

$$\frac{\mathrm{d}Y_i}{\mathrm{d}x} = \frac{\dot{\omega}_i M W_i}{\rho U} + \frac{1}{\dot{m}}\frac{\mathrm{d}\dot{m}_i}{\mathrm{d}x} - \frac{Y_i}{\dot{m}}\frac{\mathrm{d}\dot{m}}{\mathrm{d}x} \tag{11}$$

$$\frac{\mathrm{d}\overline{MW}}{\mathrm{d}x} = -\overline{MW}^2\sum_i \frac{1}{MW_i}\frac{\mathrm{d}Y_i}{\mathrm{d}x} \tag{12}$$

$$\frac{\mathrm{d}U}{\mathrm{d}x} = \frac{1}{\alpha}\left\{-\frac{\gamma M^2}{2}\left(\frac{4C_f}{D}\right) - \left[\gamma M^2 + 1 - \frac{h_o}{\overline{h_o}}\right]\frac{1}{\dot{m}}\frac{\mathrm{d}\dot{m}}{\mathrm{d}x} + \frac{1}{\overline{MW}}\frac{\mathrm{d}\overline{MW}}{\mathrm{d}x} + \frac{1}{A}\frac{\mathrm{d}A}{\mathrm{d}x} + \left(\sum_i h_i\frac{\mathrm{d}Y_i}{\mathrm{d}x}\right)\Big/\overline{h_o} + \frac{1}{\dot{m}\overline{h_o}}\frac{\mathrm{d}[\dot{Q}''A]}{\mathrm{d}x} - \frac{1}{\dot{m}\overline{h_o}}\left[\sum_i h_i\left(\dot{m}_i\frac{\mathrm{d}Y_i}{\mathrm{d}x} + \frac{\mathrm{d}\dot{m}_i}{\mathrm{d}x}\right)\right]_{\text{added}}\right\} \tag{13}$$

$$\frac{\mathrm{d}\rho}{\mathrm{d}x} = \rho\left[\frac{1}{\dot{m}}\frac{\mathrm{d}\dot{m}}{\mathrm{d}x} - \frac{1}{U}\frac{\mathrm{d}U}{\mathrm{d}x} - \frac{1}{A}\frac{\mathrm{d}A}{\mathrm{d}x}\right] \tag{14}$$

$$\frac{\mathrm{d}p}{\mathrm{d}x} = -\gamma p M^2\left[\frac{1}{U}\frac{\mathrm{d}U}{\mathrm{d}x} + \frac{1}{2}\left(\frac{4C_f}{D}\right) + \frac{1}{\dot{m}}\frac{\mathrm{d}\dot{m}}{\mathrm{d}x}\right] \tag{15}$$

$$\frac{\mathrm{d}T}{\mathrm{d}x} = T\left[\frac{1}{p}\frac{\mathrm{d}p}{\mathrm{d}x} - \frac{1}{\rho}\frac{\mathrm{d}\rho}{\mathrm{d}x} + \frac{1}{\overline{MW}}\frac{\mathrm{d}\overline{MW}}{\mathrm{d}x}\right] \tag{16}$$

where

$$\alpha \equiv \frac{1}{U}\left[\gamma M^2 - 1 - \frac{U^2}{\overline{h_o}}\right] \tag{17}$$

and

$$\overline{h_o} \equiv \left(c_p - \frac{\left[\sum_i \dot{m}_i c_{p_i}\right]_{\text{added}}}{\dot{m}}\right)T \tag{18}$$

The combustor model shown by Eqs. (11–18) was validated by O'Brien and Lewis[18] using experimental results by Billig and Grenleski[19] and Anderson and Gooderum.[20] The terms shown by Eqs. (11–18) form a stiff set of ordinary differential equations (ODEs); a result of the chemical production terms. To solve this set of equations, a stiff ODE solver, which could account for differing timescales, was used (a code named VODPK,[21] developed by Lawrence Livermore National Lab.). VODPK uses a backward-differencing formula to integrate the set of stiff ODEs. Values for the individual chemical species molecular weight, specific heat, and reaction rates are supplied by CHEMKIN-II[22] for a user-supplied reaction mechanism. The Jet-A reaction mechanism used for this study is a subset of the full reaction mechanism from Kundu et al.[23] The reduced mechanism consists of 17 species and 14 reactions and was chosen because it has been thoroughly validated by Chang[24] and Lewis and Chang.[25] This smaller reaction set allows for increased computational savings when combined into the optimization package.

The injection model used for this study was created from a curve fit[18] of empirical data for normal injection of hydrogen[26] fuel

$$\phi_{\text{inj}} = \phi \frac{b\bar{x}^a e^{c\bar{x}}}{d\bar{x} + f} \tag{19}$$

$$\bar{x} \equiv \frac{x - X_{\text{inj}_s}}{X_{\text{inj}_e} - X_{\text{inj}_s}} \tag{20}$$

where ϕ_{inj} is the fraction of the equivalence ratio ϕ, which has been injected. The curve-fit constants are $a = 0.62925, b = 1.1703, c = 0.42632, d = 1.4615$, and $f = 0.32655$. The variables X_{inj_s} and X_{inj_e} are the start (s) and end (e) of the fuel injectors, respectively, as was shown in Fig. 4. The values of $\bar{x}$ in Eq. (19) are only valid between X_{inj_s} and X_{inj_e}. For $x < X_{\text{inj}_s}$ the injected fuel fraction is $\phi_{\text{inj}} = 0$, and for $x > X_{\text{inj}_e}$ all of the fuel has been injected, $\phi_{\text{inj}} = \phi$. This injection model merely provides an estimate for a mass addition profile and is not used to simulate the actual combustible fuel profile because hydrocarbon mixing properties will be vastly different from that of hydrogen.

Also incorporated into this model are the flexibility of introducing a mixing length L_{mix} and mixing efficiency η_{mix}. The mixing efficiency is applied globally to the combustor flowfield in an attempt to model fuel droplets of excess size that add mass to the system, but never achieve a combustible state. This effectively allows the combustor to carry the extra fuel mass through the computation while still accounting for the thermodynamic effects of its presence. The mixing length is applied incrementally to the fuel added between X_{inj_s} and X_{inj_e} to allow the fuel sufficient length to mix and achieve a combustible state. Therefore, the fuel injected first achieves a combustible state at a length of $x = X_{\text{inj}_s} + L_{\text{mix}}$ with the fuel injected last achieving a combustible state at $x = X_{\text{inj}_e} + L_{\text{mix}}$. This combustible fuel does not include the inert fuel because of a nonideal mixing efficiency η_{mix}. Figure 7 shows the fuel mass fraction results of a sample combustor with the various injection and mixing regions labeled for clarity.

To solve the set of ODEs shown in Eqs. (11–18) for the scramjet flowfield properties, a marching procedure is used down the length of the combustor. The solution procedure at each step begins by solving Eq. (11) for the conservation of each species used in the reaction mechanism. The mass addition rates are known by the injection model shown in Eq. (19), and the chemical production rates $\dot{\omega}_i$ are determined by CHEMKIN-II. The solution of the species mass fraction in Eq. (11) then leads directly to the solution of Eq. (12) for the molecular weight of the mixture. Using the known mass injection, area, and heat-transfer distributions along with the solutions for the species mass fraction and mixture molecular weight, the velocity distribution in Eq. (13) can be solved. The value for the skin-friction coefficient is assumed to be turbulent for the combustor.[12] Gas constants at each step of the combustor are calculated using CHEMKIN-II. The wall heat-transfer coefficient in Eq. (13) is determined using Reynolds Analogy with the adiabatic

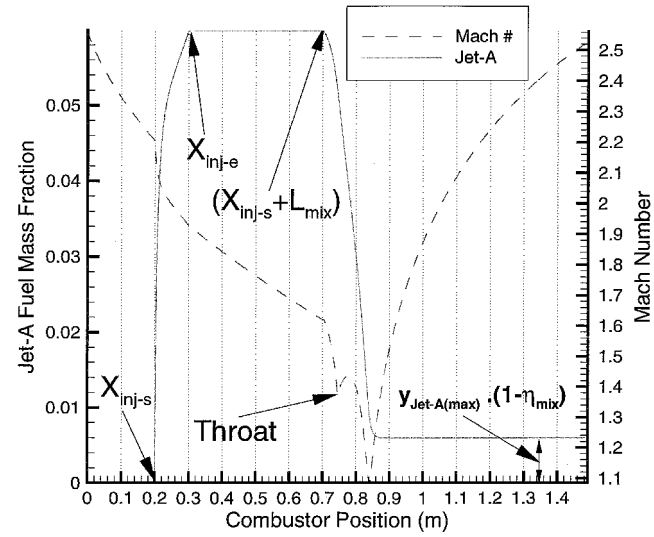

Fig. 7 Fuel mass fractions for sample injection and mixing profiles.

wall temperature

$$T_{\text{aw}} = T\left[1 + Pr^{\frac{1}{3}}\frac{(\gamma - 1)M^2}{2}\right] \tag{21}$$

and using the Prandtl number Pr for air of 0.71. The heat-transfer coefficient is

$$\frac{\mathrm{d}Q}{\mathrm{d}x} = \frac{2C_f c_{p_m}(T_{\text{aw}} - T_w)}{Pr^{\frac{2}{3}} D} \tag{22}$$

where the hydraulic diameter is

$$D = 4\,\mathrm{d}x\frac{A_w}{\mathrm{d}A_w} \tag{23}$$

and c_{p_m} is the specific heat at constant pressure for the mixture (m). Knowing the solution to the velocity derivative, the solutions to Eqs. (14–16) can be readily calculated for density, pressure, and temperature, respectively.

Optimization

Optimization of these missile geometries was difficult because of the internal and external constraints, as well as the nonlinear nature of high-speed aerodynamics and sensitivity of scramjet engines. Varying the magnitudes of many of the design variables by small amounts often changed an ideal missile configuration into one that was geometrically infeasible, nonrealistic, or nonfunctioning (i.e., insufficient propulsion or choked flow). These problems became insurmountable when using a gradient-based optimizer. The major problem is that the robust gradient methodologies require initializing and remaining mainly within the feasible design space (i.e., no gradient information can be generated for infeasible designs). Also, because the design space for this missile is highly nonlinear and discontinuous (i.e., multiple local optima separated by infeasible regions) and discrete design variables were necessary a genetic-algorithm (GA)-based optimization methodology was a logical solution.

In the simplest sense a genetic algorithm is a random number based trial-and-error approach to optimization.[27,28] A genetic algorithm does not need an initial guess to begin the process, rather it starts with a population of initial solutions and then selects the best performers to survive and then reproduce. Once the objective functions have been calculated for an entire generation of configurations, the GA examines the statistics for the entire population and then determines the survivors through a tournament selection process (i.e., randomly picking pairs of chromosomes where the one with better overall performance for the objective functions survives). After this, the survivors are allowed to cross over and mutate

to determine the offspring. This process continues until an optimum, or sufficiently optimum, solution is found.

A pareto-based evolutionary optimization is performed using a parallelized, floating-point based, GA package developed for this study.[8] Pareto-optimal solutions are given by chromosomes that dominate all others for all objective functions, the elite solutions. Multiple objective functions are solved for simultaneously, and the relative performance of each is determined. This allows for the most critical design objective to be given the highest priority when determining the fittest chromosomes for reproduction. The GA software was written to utilize Parallel Virtual Machine,[29] a publicly available code, to enable multicomputer, multiarchitecture, parallelization. Solutions took between 250,000 and 600,000 function calls (individual vehicle designs). Initial, or primer, populations with which to start the GA were built using 100,000 function calls for the single-engine designs and 250,000 function calls for the double-engine designs. The actual number of suboptimal vehicles designs generated from these primer sets (i.e., designs which could be solved tip-to-tail without violating a constraint) was on the order of 0.5% for single-engine missiles and 0.1% for double-engine missiles. This way the optimizations were started using as many feasible designs as possible. Violated constraints were considered anything for which the vehicle calculations could not be completed, such as choked engine flow, having the planar part of forebody shock not as wide as the engine, geometric constraints exceeded, etc.

Objective Functions

Because of the pareto nature of the optimization package, numerous objective functions can be solved simultaneously and given weightings in order to determine an overall chromosome fitness. Every chromosome that results in a complete vehicle design is rated according to the following objective functions (in order of importance):

1) *Translational acceleration* (a_x): Because no trajectory analysis has been included in this present work, thrust is set equal to drag at the beginning of the cruise altitude (i.e., zero angle of attack).

$$a_x = (T - D_w - D_v)/m \tag{24}$$

2) *Vertical acceleration* (a_z): The net lift at cruise altitude was constrained to be equal to the initial cruising weight of the missile.

$$a_z = (L_p + L_{\text{cen}} - W)/m \tag{25}$$

3) *Angular acceleration* (ω): To achieve a steady-state cruise condition, zero pitching moment about the center of gravity was desired at zero degree angle of attack.

$$\omega = \sum M_{C_g} \Big/ I_y \tag{26}$$

4) *Cruise range* (R): The design point used for this study is to achieve a steady-state trimmed design at the beginning of the cruising part of its trajectory. The overall objective of this study is to maximize the range of the missile at cruise altitude using the Brueget range equation (assuming that no fuel has been used in reaching cruise altitude).

$$R = U_\infty I_{\text{sp}} \left(\frac{L_p + L_{\text{cen}}}{D_w + D_v} \right) \ln \left(\frac{m_s + m_f}{m_s} \right) \tag{27}$$

Although the Brueget range equation assumes a constant value of the vehicle lift-to-drag ratio, the error introduced for these integrated missile configurations is minimal because of their low overall values of L/D (between about 0.5 and 1.9). The Brueget equation provides a simple range evaluation with minimal effort. The desired 750-km cruise range for these missiles results in a cruise flight time of about 5 min at Mach 8. Because Eq. (27) is only valid for $T = D$ and $L = W$ conditions, the final objective function was only assigned a value if the other three objective functions were within specified tolerances. If the first three functions were not close to the cruise conditions, the resulting range would be grossly exaggerated causing the optimization to diverge.

A volumetric efficiency based on box size $\eta_{\text{box}} = V/V_{\text{box}} = V/1.59\ \text{m}^3$ is used as a figure of merit to determine how well the available box size is utilized up by each configuration. The missile range should be maximized to some degree by filling the box size as much as possible. For the vehicles reported in this study, the volume used is the structural and internal volume. The volume internal to the scramjet engines is assumed to be lost and is not included in this figure of merit.

Results

The parametric study contained herein varies the magnitudes of the design parameters for which reasonable approximations are unknown. This effort helps to resolve the bounding box of the feasible design space and determine the most sensitive design parameters. Some of the design points are optimistic whereas others are penalizing. The fuel volume fraction κ, fuel mixing and burning efficiency η_{mix}, mixing length L_{mix}, and fuel injector starting and ending locations X_{inj_s} and X_{inj_e} were deemed the most critical design parameters for this study. Six different cases were optimized for maximum cruise range with either one or two engines using $\eta_{\text{mix}} = 90$ or 100% and $\kappa = 25$ or 50%. The resulting missiles from these various design points are shown in Figs. 8–13, with the optimization details shown in Table 1.

Optimization Study

By lowering the mixing efficiency by only 10%, the resulting optimization shown in case 1 ($\eta_{\text{mix}} = 90\%$) actually achieved a farther range than the ideal engine optimization shown in case 3

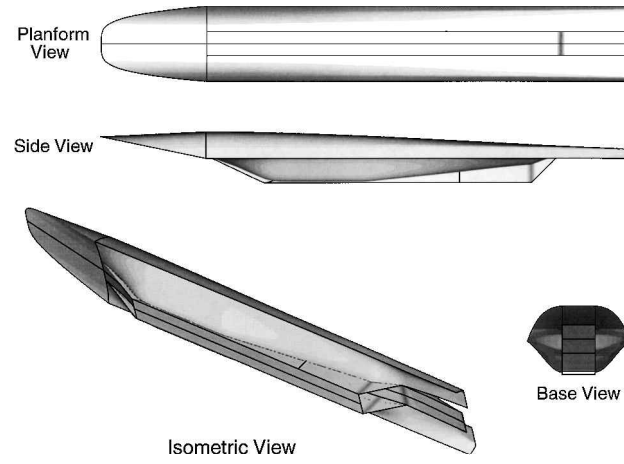

Fig. 8 Case 1: $\eta_{\text{mix}} = 90\%$, $\kappa = 25\%$.

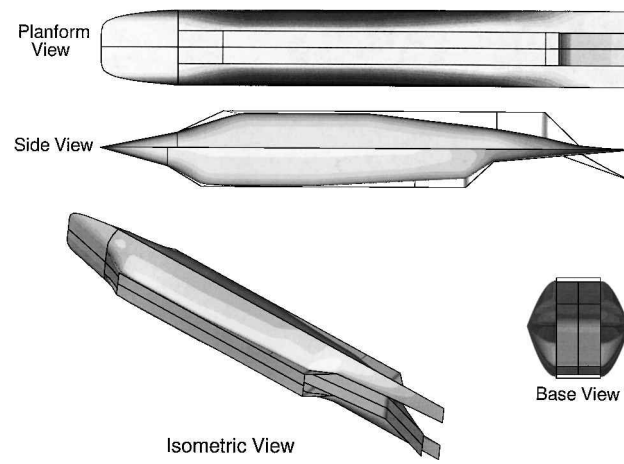

Fig. 9 Case 2: $\eta_{\text{mix}} = 90\%$, $\kappa = 25\%$.

Table 1 Optimized missile results. (Baseline values: $M = 8$, $L_{mix} = 0.5$ m, $X_{inj} = 0.2$ m $\rightarrow$ 0.3 m)

	$\eta_{mix} = 90\%$		$\eta_{mix} = 100\%$			
	$\kappa = 25\%$		$\kappa = 25\%$		$\kappa = 50\%$	
Parameters	1 Engine (Case 1)	2 Engines (Case 2)	1 Engine (Case 3)	2 Engines (Case 4)	1 Engine (Case 5)	2 Engines (Case 6)
Geometric parameters						
Ramps	2	1, 1	2	2, 3	2	3, 2
Fuel mass, kg	84	143	98	141	196	296
Missile mass, kg	547	816	563	841	660	918
π_f	0.154	0.175	0.174	0.168	0.297	0.322
S_{cap}, cm^2	720	830, 780	757	711, 807	654	745, 742
S_{inlet}, cm^2	32.2	58.2, 62.4	31.2	37.2, 41.4	32.9	57.1, 47.1
η_{box}	0.264	0.444	0.303	0.439	0.305	0.456
h, m	0.41	0.61	0.45	0.61	0.44	0.61
Z, km	31.8	28.9	30.8	26.2	28.5	23.4
R, km	**1432**	**696**	**1297**	**1094**	**2340**	**1637**
Aerodynamic parameters						
L, N	5595	8337	5794	8615	6817	9444
D_w, N	1729	5366	2360	5229	2523	8118
D_v, N	1137	3047	1388	4684	1583	6070
L/D	1.864	0.947	1.477	0.831	1.587	0.637
Combustor parameters						
p_{inlet}, atm	1.52	1.44, 0.87	2.37	2.43, 2.35	2.07	2.81, 2.80
T_{inlet}, K	1335	1283, 968	1482	1112, 1067	1261	1183, 1023
$\dot{m}_a$, kg/s	2.44	4.35, 4.09	3.00	5.67, 6.43	3.637	9.16, 9.13
$\dot{m}_f$, kg/s	0.15	0.24, 0.30	0.20	0.12, 0.22	0.24	0.23, 0.29
ϕ	0.93	0.84, 1.12	1.00	0.32, 0.51	0.99	0.38, 0.48
T, N	**2868**	**4026, 4408**	**3733**	**4116, 5780**	**4115**	**6240, 7918**

Table 2 Perturbation study results. (Baseline values: $M = 8$, $L_{mix} = 0.5$ m, $X_{inj} = 0.2$ m $\rightarrow$ 0.3 m)

	Change in missile thrust, N [% thrust lost]					
	$\eta_{mix} = 90\%$		$\eta_{mix} = 100\%$			
	$\kappa = 25\%$		$\kappa = 25\%$		$\kappa = 50\%$	
Parameters	1 Engine (Case 1)	2 Engines (Case 2)	1 Engine (Case 3)	2 Engines (Case 4)	1 Engine (Case 5)	2 Engines (Case 6)
$L_{mix} = 0.45$ m	choked [-]	choked [-]	choked [-]	choked [-]	choked [-]	choked [-]
$L_{mix} = 0.55$ m	−1355 [47.2]	−1460, −1742 [38.0]	−1617 [43.3]	−394, −1832 [22.5]	−1963 [47.7]	−374, −128 [3.5]
$X_{inj} = 0.15$ m $\rightarrow 0.25$ m	choked [-]	choked [-]	choked [-]	choked [-]	choked [-]	choked [-]
$X_{inj} = 0.25$ m $\rightarrow 0.35$ m	−1348 [47.0]	−1436, −1474 [34.5]	−1607 [43.0]	−354, −1762 [21.4]	−1951 [47.4]	−317, −107 [3.0]
$\eta_{mix} = 85\%$	−518 [18.1]	−746, −2187 [34.8]	−1266 [33.9]	−360, −1271 [16.5]	−1573 [38.2]	−644, −634 [9.0]
$\eta_{mix} = 95\%$	choked [-]	choked [-]	−777 [20.8]	−130, −251 [3.9]	−1140 [27.7]	−183, −191 [2.6]

($\eta_{mix} = 100\%$). This increase in range can be attributed to many differences between the cases. Because optimization case 1 was required to pass unburned fuel through its combustor, it required a slightly larger inlet area and utilized a substantially lower inlet pressure. Interestingly, the engine used by the missile in case 1 produced the least thrust of all of the cases, which in turn required it to be coupled to the most aerodynamically efficient geometry. Correspondingly, the optimized geometry in case 1 had the lowest box efficiency (i.e., volume) and fuel mass fraction of all of the cases. Because case 1 had about the same weight as case 3, the fact that it was able to generate a better lifting body with less drag at a higher altitude indicates the importance of investigating the effects of coupled engine/airframe systems together. The overall result was that case 1, as a result of a poorer engine, required a much more slender body with lower drag and higher L/D than in case 3.

Although the 10% improvement in optimized cruise range for case 1 over case 3 is substantial, the more noteworthy result is that the best engine (case 3) did not produce the best range (case 1) for the single-engine designs. Rather, the performance of the engine was highly coupled to the airframe, which was delivering the required inlet conditions. This provides an interesting quandary for engine designers and developers; because the best engine (in this restrictive missile design environment) does not guarantee the best integrated performance, what engine design conditions should be used?

This same trend in cruise range did not hold for the two engine missiles in cases 2 and 4 for changing the mixing efficiency by 10%. The two engine configurations encountered more difficulty generating the lift necessary to match their weight. Although case 2 also increased its altitude and lowered its inlet pressures compared to case 4, the resulting range was poor because of an overconstrained engine geometry. This is shown by the extremely large control surface deflection needed to generate lift and trim the vehicle moment, as shown in Fig. 9. Case 4 also had a fairly large control surface deflection, but did not have as much moment to trim because its engines were of similar size and position. By designing the combustor with the throat always in the middle, the two engine configurations did not have enough flexibility in the design space, resulting in poor designs.

Cases 1–4 were all optimized using an estimated fuel volume fraction of 25%; a reasonable assumption for the single-engine vehicles.

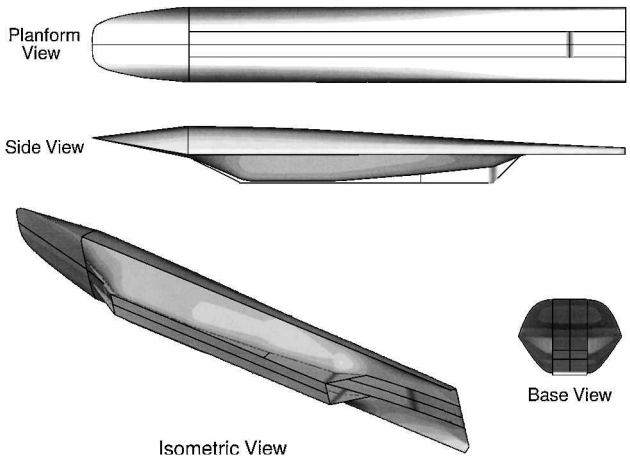

Fig. 10 Case 3: $\eta_{mix} = 100\%, \kappa = 25\%$.

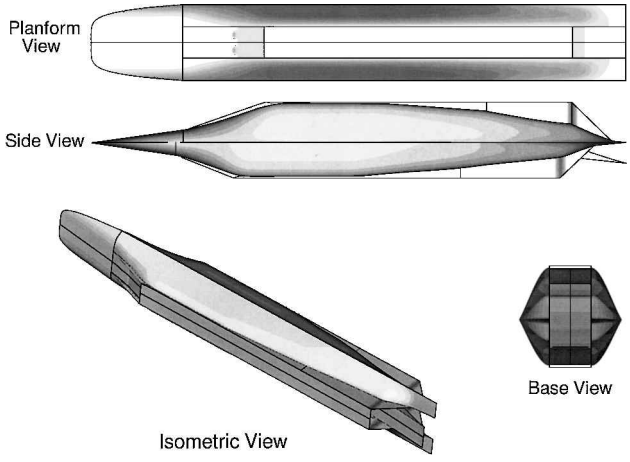

Fig. 11 Case 4: $\eta_{mix} = 100\%, \kappa = 25\%$.

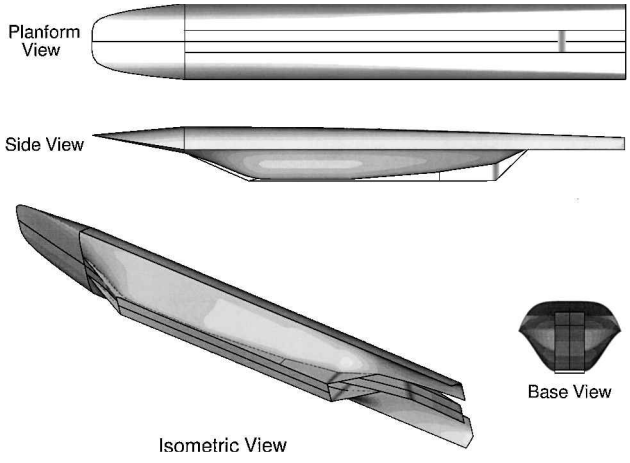

Fig. 12 Case 5: $\eta_{mix} = 100\%, \kappa = 50\%$.

This assumption is penalizing for the two engine vehicles because the subsystem weight and size would be similar to the one engine vehicles. The result is that the two engine missiles would have a larger fuel volume fraction than the single-engine missiles; closer to the $\kappa = 50\%$ estimate used for cases 5 and 6. The ranges for cases 5 and 6 show a dramatic increase over cases 1 through 4, but still leave room for uncertainty of which configuration is superior (i.e., one or two engines) and which assumption set carries the most credibility. However, cases 5 and 6 allow for insight into what can be gained by having heavier missiles with more fuel available.

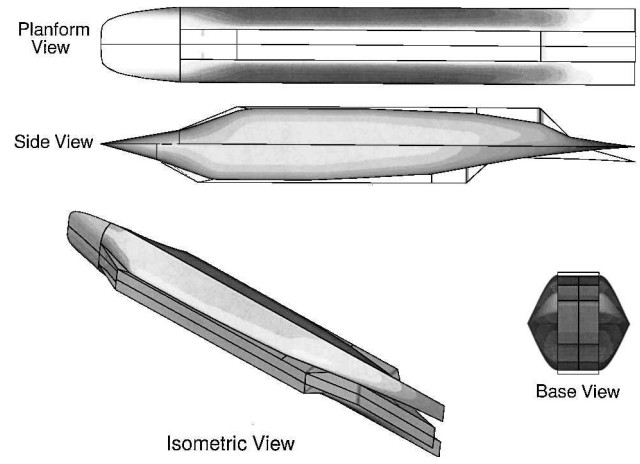

Fig. 13 Case 6: $\eta_{mix} = 100\%, \kappa = 50\%$.

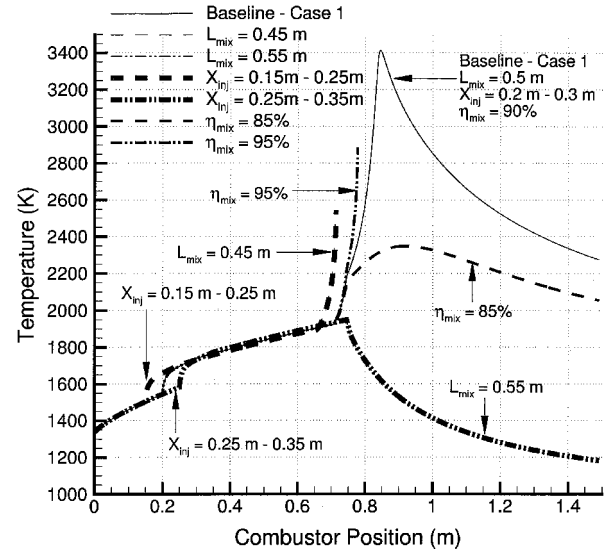

Fig. 14 Combustor temperature profiles for missile case 1.

Perturbation Study

The missiles shown in Figs. 8–13 were all optimized for unique design points. This was to determine the effects combustion properties would have on vehicles optimized for maximum range. The next goal of this study was to see what the effect of errors in the assumed values for mixing length L_{mix}, fuel-injector location X_{inj}, and fuel mixing efficiency η_{mix} would have on the optimized missile designs. By perturbing the design point of each optimization in cases 1 through 6, the effects of small unknowns in the design variables were quantified and were shown to have a large impact on the vehicle thrust, as shown by the results in the bottom half of Table 2.

There were a number of different design perturbations that caused thermal choking in the designs presented. The effect of lowering the mixing length caused all of the engines to choke, as did moving the injector locations 5 cm closer to the front of the engine. Cases 1 and 2 also choked for an increase in mixing efficiency. The reason for the thermal choking in these engines is because they were all designed (optimized) in such a manner that required the fuel ignition to begin very close to the throat so that the flow could expand in the diverging section to avoid choking. Any changes in the flowfield affected the delicate blend of heat addition through combustion and cooling through expansion, as shown in the temperature profiles for case 1 in Fig. 14.

For the remainder of the perturbations where thermal choking did not occur, substantial penalties in the amount of thrust generated are noted (up to 48%). These design sensitivities are also understood by the temperature profiles shown in Fig. 14. By optimizing the

missiles for realistic cruise designs points, not enough flexibility was left in the designs for fluctuations in the flowfield because they all designed to operate at peak performance.

The largest and heaviest missile (case 6) showed the least sensitivity to changes in the combustor variables. Where other configurations had significant thrust losses for most or all perturbations tested, case 6 had a peak thrust loss of 9% for the test where the mixing efficiency was dropped from 100 to 85%. Because of its weight, case 6 had the lowest cruising altitude and highest inlet pressures of all of the cases. Also, case 6 optimized with the highest air mass flow rates and lowest equivalence ratios of all the cases. Case 6 required the most thrust of all of the cases and had the lowest L/D ratio.

These perturbation results indicate that a more robust engine design can be found by a combination of higher inlet pressure, higher air mass flow rate, and a lower equivalence ratio. Comparatively, the single-engine designs had much more sensitivity to the changes in the combustor flowfield than the double-engine cases.

Conclusions

The optimized single- and double-engine missiles configurations were all shown to have noticeable differences for each of the different design points and also for perturbations of the combustion variables around those design points. The effects of chemistry add a new element to both optimization and design point selection as a result of the extremely sensitive and sudden nature of the fuel ignition process. The effects of uncertainty in design variables cause extremely undesirable changes in the performance characteristics, most noticeably for the single-engine designs. Decreased sensitivity to flowfield perturbations could be found by designing the engine for optimum conditions, $\eta_{\text{mix}} = 100\%$, $X_{\text{inj}_s} = X_{\text{inj}_e} = 0$ m, and $L_{\text{mix}} = 0$ m, and operating them suboptimally. Theoretically, by allowing the engine this capability of handling higher mass flow rates the loss of peak performance (on design) would be balanced by the minimization the off-design performance degradation. By designing the engine assuming ignition at the earliest possible location in the combustor, any changes in the flowfield could only cause the ignition to move further downstream, possibly avoiding choking. It is uncertain whether or not this would prohibit ignition caused by freezing of the flow at the combustor throat.

In addition to the engine requirements for a integrated hypersonic missile, it was also noted that through the use of suboptimal engine performance ($\eta_{\text{mix}} = 90\%$) more efficient aerodynamic geometries can be realized. By integrating this effect with the preceding engine design insights, better airframes could be designed to be coupled with the engines. Overall, the best engine design for a given set of conditions does not necessarily ensure the best overall vehicle performance.

Acknowledgments

This research was supported by the Center for Hypersonic Education and Research at the University of Maryland under technical monitor Isaiah Blankson of NASA (NASA Grant NAGw 11796), the support of whom is greatly appreciated.

References

[1]Starkey, R. P., and Lewis, M. J., "Critical Design Issues for Airbreathing Hypersonic Waverider Missiles," *Journal of Spacecraft and Rockets*, Vol. 38, No. 5, 2001, pp. 510–519.

[2]Nonweiler, T. R. F., "Aerodynamic Problems of Manned Space Vehicles," *Journal of the Royal Aeronautical Society*, Vol. 63, Sept. 1959, pp. 521–528.

[3]Center, K. B., Sobieczky, H., and Dougherty, F. C., "Interactive Design of Hypersonic Waverider Geometries," AIAA Paper 91-1697, June 1991.

[4]Takashima, N., and Lewis, M. J., "Navier–Stokes Computation of a Viscous Optimized Waverider," AIAA Paper 92-0305, Jan. 1992.

[5]Gillum, M. J., and Lewis, M. J., "Experimental Results on a Mach 14 Waverider with Blunt Leading Edges," *Journal of Aircraft*, Vol. 34, No. 3, 1997, pp. 296–303.

[6]Starkey, R. P., and Lewis, M. J., "Simple Analytical Model for Parametric Studies of Hypersonic Waveriders," *Journal of Spacecraft and Rockets*, Vol. 36, No. 4, 1999, pp. 516–523.

[7]Starkey, R. P., "A Parametric Study of L/D and Volumetric Efficiency Trade-Offs for Waverider Based Vehicles," M.S. Thesis, Dept. of Aerospace Engineering, Univ. of Maryland, College Park, June 1998.

[8]Starkey, R. P., "Investigation of Air-Breathing, Hypersonic Missile Configurations Within External Box Constraints," Ph.D. Dissertation, Dept. of Aerospace Engineering, Univ. of Maryland, College Park, Oct. 2000.

[9]Anderson, J. D., *Modern Compressible Flow: with Historical Perspective*, McGraw–Hill, New York, 1990.

[10]Anderson, J. D., *Hypersonic and High Temperature Gas Dynamics*, McGraw–Hill, New York, 1989.

[11]Taylor, G. I., and Maccoll, J. W., "The Air Pressure on a Cone Moving at High Speed," *Proceedings of the Royal Society of London*, Vol. 139, 1933, pp. 278–311.

[12]White, F. M., *Viscous Fluid Flow*, 2nd ed., McGraw–Hill, New York, 1991.

[13]Bowcutt, K., Anderson, J., and Capriotti, D., "The Viscous Optimized Hypersonic Waveriders," AIAA Paper 87-0272, 1987.

[14]Waltrup, P. J., White, M. E., Zarlingo, F., and Gravlin, E. S., "History of U.S. Navy Ramjet, Scramjet, and Mixed-Cycle Propulsion Development," AIAA Paper 96-3152, 1996.

[15]O'Brien, T., Starkey, R. P., and Lewis, M. J., "A Quasi-One-Dimensional High-Speed Engine Model with Finite-Rate Chemistry," *Journal of Propulsiona and Power*, Vol. 17, No. 6, 2001, pp. 1366–1374.

[16]Shapiro, A. H., *The Dynamics and Thermodynamics of Compressible Fluid Flow*, Vol. 1, McGraw–Hill, New York, 1953.

[17]Turns, S. R., *An Introduction to Combustion*, McGraw–Hill, New York, 1996.

[18]O'Brien, T., and Lewis, M. J., "RBCC Engine-Airframe Integration on an Osculating Cone Waverider Vehicle," AIAA Paper 2000-3823, July 2000.

[19]Billig, F. S., and Grenleski, S. E., "Heat Transfer in Supersonic Combustion Processes," *Heat Transfer 1970*, Vol. III, Elsevier, 1970.

[20]Anderson, G. Y., and Gooderum, P. B., "Exploratory Tests of Two Strut Fuel Injectors for Supersonic Combustion," NASA TN D-7581, 1974.

[21]Byrne, G. D., Hindmarch, A. C., and Brown, P. N., "VODPK: Variable-Coefficient Ordinary Differential Equation Solver with the Preconditioned Krylov Method GMRES for the Solution of Linear Systems," Lawrence Livermore National Lab., Livermore, CA, 1997.

[22]Kee, R. J., Rupley, F. M., and Miller, J. A., "Chemkin-II: A Fortran Chemical Kinetics Package for the Analysis of Gas Phase Chemical Kinetics," SAND 89-8009B, Sandia National Labs., Livermore, CA, 1989.

[23]Kundu, K. P., Penko, P. F., and Yang, S. L., "Reduced Reaction Mechanisms for Numerical Calculations in Combustion of Hydrocarbon Fuels," AIAA Paper 98-0803, Jan. 1998.

[24]Chang, J. S., "Development of a Jet-A/Silane/Hydrogen Reaction Mechanism for Modeling a Scramjet Combustor," Scholarly Paper, Dept. of Aerospace Engineering, Univ. of Maryland, College Park, 1999.

[25]Lewis, M. J., and Chang, J. S., "Joint Jet-A/Silane/Hydrogen Reaction Mechanism," *Journal of Propulsion and Power*, Vol. 16, No. 2, 2000, pp. 365–367.

[26]Rogers, R. C., "Mixing of Hydrogen Injected from multiple Injectors Normal ot a Supersonic Airstream," NASA TN D-6476, 1971.

[27]Goldberg, D. E., *Genetic Algorithms in Search, Optimization, and Machine Learning*, Addison Wesley Longman, Reading, MA, 1989.

[28]Michalewicz, Z., *Genetic Algorithms + Data Structures = Evolution Programs*, Springer-Verlag, New York, 1996.

[29]Geist, A., Beguelin, A., Dongarra, J., Jiang, W., Manchek, R., and Sunderam, V., *PVM: Parrallel Virtual Machine—A User's Guide and Tutorial for Networked Parallel Computing*, MIT Press, London, 1994.